Strain, electric-field and functionalization induced widely tunable electronic properties in MoS2/BC3, /C3N and / C3N4 van der Waals heterostructures

Nanotechnology

ACCEPTED MANUSCRIPT

Strain, electric-field and functionalization induced widely tunable electronic properties in MoS2/BC3 , /C3N and /C3N4 van der Waals heterostructures

To cite this article before publication: Asadollah Bafekry *et al* 2020 *Nanotechnology* in press https://doi.org/10.1088/1361-6528/ab884e

Strain, electric-field and functionalization induced widely tunable electronic properties in MoS_2/BC_3, $/C_3N$ and $/C_3N_4$ van der Waals heterostructures

A. Bafekry,[1,2,*] C. Stampfl,[3] and M. Ghergherehchi[4,†]

[1] *Department of Physics, University of Guilan, 41335-1914 Rasht, Iran*
[2] *Department of Physics, University of Antwerp, Groenenborgerlaan 171, B-2020 Antwerp, Belgium*
[3] *School of Physics, The University of Sydney, New South Wales 2006, Australia*
[4] *College of Electronic and Electrical Engineering, Sungkyun kwan University, Suwon, Korea*

In this paper, the effect of BC_3, C_3N and C_3N_4 substrates on the atomic and electronic properties of MoS_2 were systematically investigated using first-principles calculations. Our results show that the MoS_2/BC_3 and MoS_2/C_3N4 heterostructures are direct semiconductors with band gaps of 0.4 and 1.74 eV, respectively, while MoS_2/C_3N is a metal. Furthermore, the influence of strain and electric field on the electronic structure of these van der Waals heterostructures is investigated. The MoS_2/BC_3 heterostructure, for strains larger than -4%, transforms it into a metal where the metallic character is maintained for strains larger than -6%. The band gap decreases with increasing strain to 0.35 eV (at +2%), while for strain ($>+6\%$) a direct-indirect band gap transition is predicted to occur. For the MoS_2/C_3N heterostructure, the metallic character persists for all strains considered. On applying an electric field, the electronic properties of MoS_2/C_3N_4 are modified and its band gap decreases as the electric field increases. Interestingly, the band gap reaches 30 meV at +0.8 V/Å, and with increase above +0.8 V/Å, a semiconductor-to-metal transition occurs. Furthermore, we investigated effects of semi- and full-hydrogenation of MoS_2/C_3N and we found that it leads to a metallic and semiconducting character, respectively.

I. INTRODUCTION

The remarkable electronic, mechanical, and optical properties of two-dimensional materials (2D) and their ability to be tuned have opened the door to their potential applications in modern electronic, catalytic, energy conversion and storage devices.[1–5] This capability has been increased by stacking of different 2DM on top of each other to form artificial heterostructures that are bound by weak van der Waals (vdW) interaction.[6–12] These vdW heterojunctions are of potential interest for 2D electronic and optoelectronic technologies due to their atomically sharp interface, absence of dangling bonds and minimal trap states. Vertical 2D devices constructed with 2D semiconductor heterostructures have shown to exhibit interesting band gaps, higher power and higher speed than traditional bulk junctions .[13,14]

Recently, a particular class of 2DM, synthesized from boron, nitrogen and carbon atoms has attracted a lot of attention due to their outstanding chemical and physical properties. Layered nanomaterials composed soley of N, C and B atoms, which can take many different positions, enhance the possibilities to form strong covalent structures. A 2D honeycomb network with stoichiometry of BC_3 has been synthesized experimentally.[15–17] By chemical synthesis, bulk BC_3 was produced which forms stacked layers that are held together by the van der Waals (vdW) interaction.[18] Monolayer BC_3 can be formed by exfoliation from the bulk counterpart, similar to the creation of graphene from graphite.[19] BC_3 shows excellent crystalline quality and has been shown to be a monolayer film.[15] Theoretical studies of BC_3 reported its electronic properties and showed that it is a semiconductor.[20–23]

2D polyaniline, with stoichiometry C_3N has a graphene-like structure.[24] Density-functional theory (DFT) calculations demonstrated that the electronic properties of C_3N can be altered by different methods such as atom adsorption and functionalization,[25–29] as well as defects.[30] Like its C_2N counterparts, C_3N is also an intrinsic semiconductor as reported in recent theoretical studies. It has been reported that monolayer C_3N shows desirable properties for different applications, including nanoelectronics, hydrogen storage and catalysis.[31–34] C_3N_4 exhibits semiconducting properties with the potential to be a photo-catalyst for water splitting.[35,36] This structure features intrinsic vacancies that may produce a spin polarized state. The electronic properties of C_3N_4 are drastically modified when atoms are substituted.[37–40] Although two-dimensional materials (2DMs) hold significant potential for many applications, it will be necessary to tune their intrinsic properties. Several approaches have been considered to change the electronic structure of 2D BCN monolayers such as substitutional doping, defect engineering, application of an electric field or strain, surface functionalization by adatoms, or by altering the edge states.[41–55,57–62,64]

In this work, by *ab initio* calculations we investigate the electronic and atomic properties of heterostructures of MoS_2 with BC_3, C_3N and C_3N_4. We show that the band gap of these heterostructures can be modified by applying an electric field and by external strain. Finally, we study the electronic properties of MoS_2/C_3N and MoS_2/C_3N_4 heterostructures under semi- and full-hydrogenation. We show that hydrogenation significantly modifies the electronic properties of these heterostructures and is able to induce metallic and semiconducting characteristics.

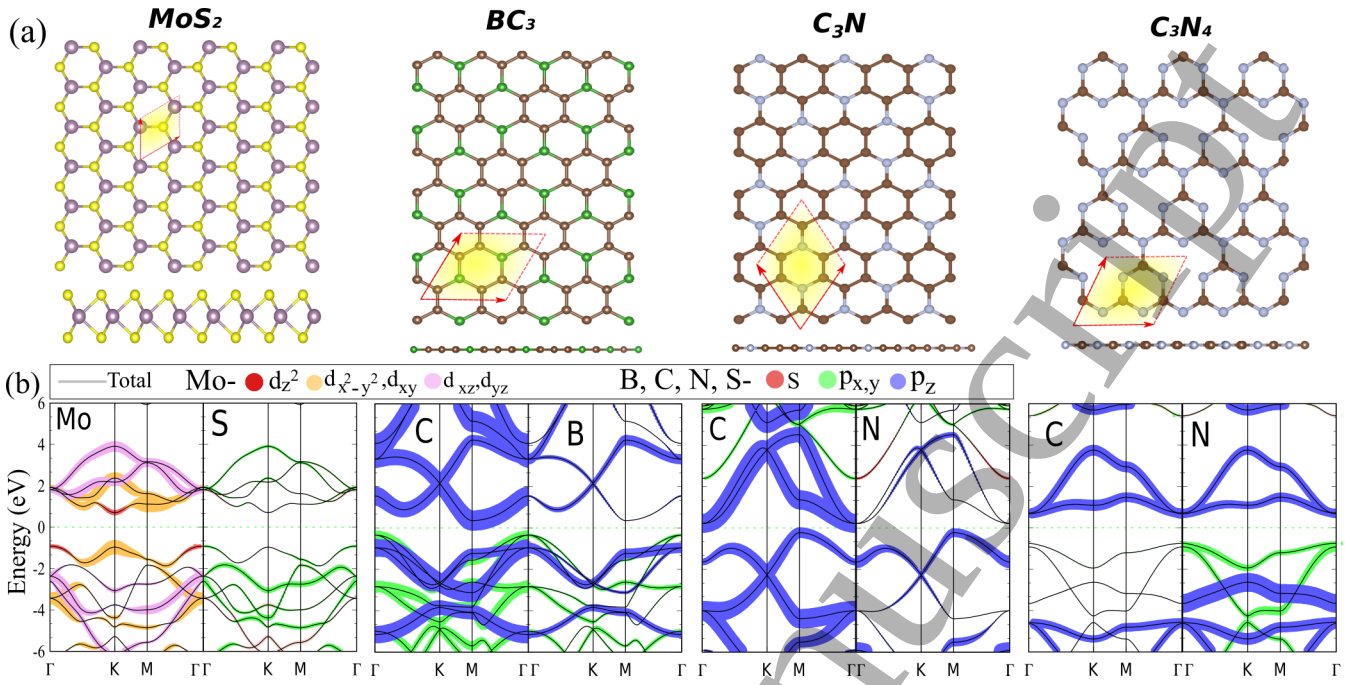

Figure 1. (a) Lattice structures and (b) calculated orbital resolved band structure of MoS_2, BC_3, C_3N and C_3N_4 monolayers. The primitive unit cell is indicated by a red parallelogram. The colors of band structures are weighted by the contributions from Mo-d orbitals: yellow lines for d_{xy} and $d_{x^2-y^2}$, red lines for d_{z^2}, and pink for d_{xz} and d_{yz}. Contributions from S-, B-, C- and N-p orbitals: blue lines for $p_{x,y}$ and blue lines for p_z. Contributions from S-, B-, C- and N-s orbital: light red lines. The zero of energy is set to the Fermi level.

II. METHOD

In this work, we report results of our spin-polarized DFT calculations for the electronic structure as implemented in the OpenMX 3.8 package.[65] This code self-consistently finds the eigenfunctions of the Kohn-Sham equations using norm-conserving pseudopotentials,[66] and pseudoatomic orbitals (PAOs).[67,68] The wave functions are expanded in a linear combination of multiple pseudoatomic orbitals (LCPAOs).[67,68] The PAO basis functions were specified by $s^2p^2d^1$ for C, B, N and S atoms, while $s^3p^2d^2$ for Mo atom within cutoff radii of basis functions set to the values of seven. We used the Perdew-Burke-Ernzerhof generalized gradient approximation (GGA) for the exchange-correlation functional.[69] The Monkhorst-Pack scheme[70] was used to generate the **k**-points for integration over the Brillouin zone (BZ) and the BZ is sampled by a mesh of $15 \times 15 \times 1$. After convergence tests, we chose different energy cutoffs (for instance 350 Ry, 400 Ry for pristine BCN monolayer and MoS_2/BCN heterostructure) so that the total-energy was converged to within 1.0 meV/atom. The atomic positions are optimized using a quasi-Newton algorithm for atomic force relaxation, where the structure was fully relaxed until the force acting on each atom was less than 1 meV/Å. The heterostructures are modelled as a periodic slab with a large vacuum region (22 Å) in order to prevent interactions between adjacent layers. To describe the vdW interactions we use the empirical correction method described by Grimme (DFT-D2).[71]

III. PRISTINE MONOLAYERS

We initially describe the atomic and electronic structure of the separate monolayers. The atomic structures of MoS_2, BC_3, C_3N and C_3N_4 monolayers are shown in Fig. 1(a). The primitive unit cell is indicated by a red parallelogram. The MoS_2 monolayer consists of three layers with the Mo layer sandwiched between two S layers. We obtain for the lattice constant 3.21 Å, the vertical S-S distance 3.19 Å and the Mo-S bond length, 2.44 Å. These results are in agreement with previous reports.[72] BC_3 has a planar structure with lattice constant 5.17 Å. The B-C and C-C bond lengths are, respectively, 1.56 and 1.42 Å, in agreement with earlier calculations.[73,74] We obtain a lattice constant of C_3N of 4.86Å, while the C-C and C-N bond lengths are 1.40 and 1.40 Å, respectively, as in agreement with previous reports.[22,24,25] After structural optimization, the lattice parameter of C_3N_4 is determined to be 4.74 Å, and the two types of bond lengths of C-N are 1.32 and 1.44 Å, respectively, while the angle of N-C-N is 117.4°, which are in agreement with a previous calculation.[75]

The orbital-resolved band structure is shown in Fig. 1(b). Notice that BC_3 is a semiconductor with an indirect band gap of 0.7 eV, in which the valence band maximum (VBM) and conduction band minimum (CBM) are

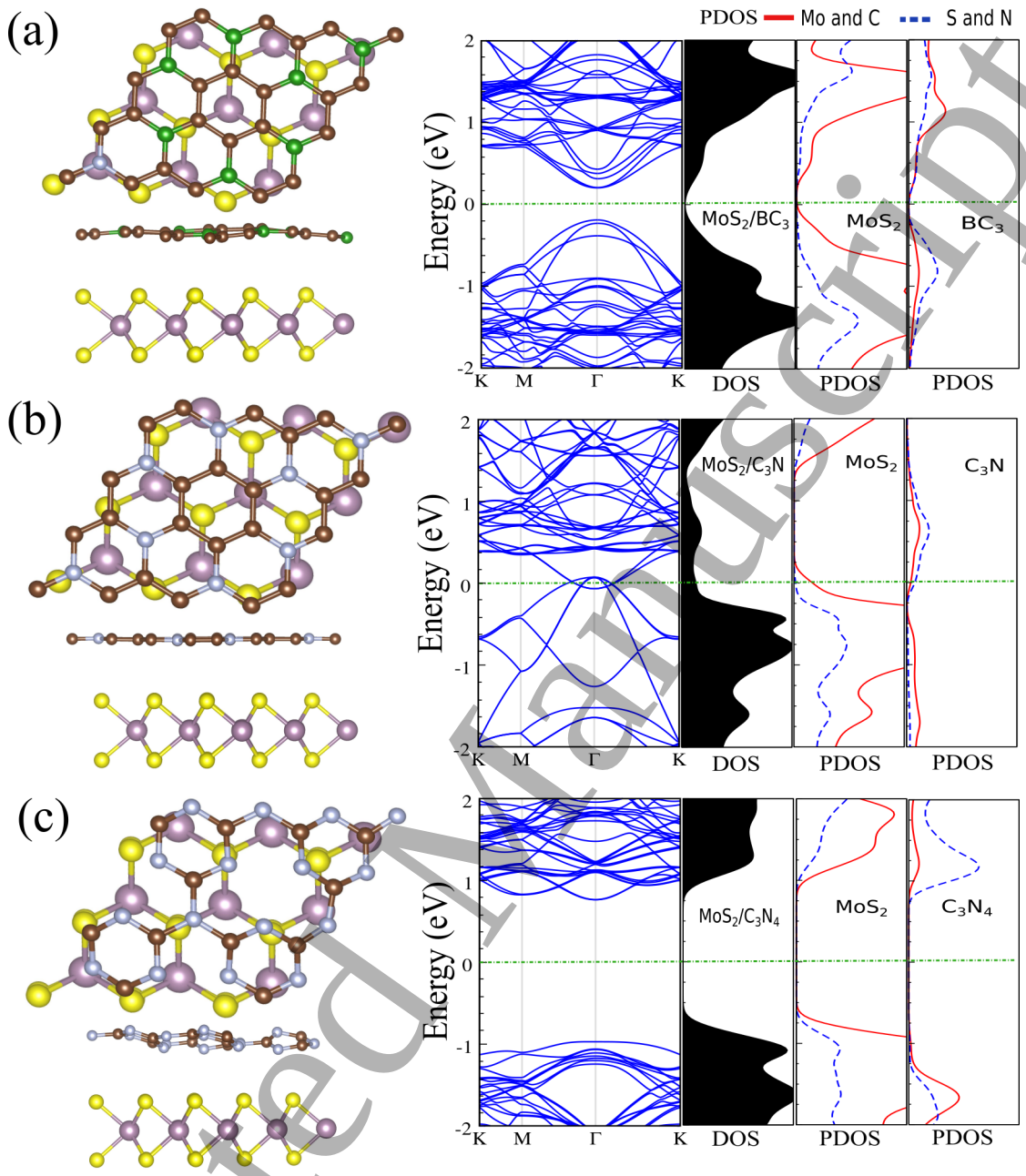

Figure 2. Top and side views of the optimized atomic structures (right panel) and electronic band structure, DOS and PDOS (left panel) of (a) MoS_2/BC_3, (b) MoS_2/C_3N and (c) MoS_2/C_3N_4 heterostructures. The zero of energy is set to the Fermi-level energy.

situated, respectively, at the Γ and M points, as found previously.[73,74] The VBM is composed of B/C-$p_{x,y}$ orbitals, and the CBM is composed of the p_z orbital between the B and C atoms. The effect of the p-orbitals can be clearly seen at the Γ point. This is very close to the s bonds at the VBM due to local distributions forming hexagonal rings. In deep energy levels, both types of s- and p-orbitals can be formed in C-C and B-C bonds. The C_3N monolayer is an indirect semiconductor with a band gap of 0.4 eV, where the CBM and VBM are located at Γ and M, respectively. From the orbital-resolved band structure, it can be seen that the VBM (CBM) originates from N-p_z (C-p_z) orbitals which is in agreement with previous studies.[24,76,78] Our results show that C_3N_4 is a direct semiconductor with a band gap of 1.45 eV and the CBM and VBM are located at Γ point. N-$p_{x,y}$ orbitals are responsible for the VBM, while N/C-p_z orbitals form the CBM, in agreement with previous reports.[35,36] We found that MoS_2 monolayer is a direct semiconductor with a band gap of 1.65 eV with both the CBM and the VBM located at the K-point.[72]

IV. PRISTINE HETEROSTRUCTURES

MoS_2 is a transition metal dicalcogenide (TMD) monolayer that has been intensively investigated during the last decade. We use this material to form heterostructures with three different boron-carbon-nitride (BCN) monolayers. For the MoS_2/BCN heterostructures, we used a 3×3 supercell of MoS_2 on top of a 2×2 supercell of BCN, while the vacuum between is take to be 22 Å in these systems. The lattice mismatch (δ) is defined as $\delta = \frac{|a_{up}-a_{dn}|}{a_{dn}} \times 100\%$, where a_{up} and a_{dn} are the lattice constants of the unrelaxed top and bottom monolayers, respectively. The lattice mismatch between MoS_2 with BC_3, C_3N, C_3N_4 monolayers are, respectively, 3.84%, 0.93% and 1.55%. Thus, relative to their free-standing structures, it is expected that there will be no major distortion in the geometric structures. We determine the lowest energy stacking configuration, including structural optimization. The different stacking patterns of MoS_2/BC_3, MoS_2/C_3N and MoS_2/C_3N_4 that we considered are shown in Fig. S1 of the supplementary information. The most stable stackings are found to be *AA* for MoS_2/BC_3, *AB* for MoS_2/C_3N and *BB* for MoS_2/C_3N_4 as the relative total energies show in Fig. S2. The structural parameters including bond length, interlayer distance and buckling are shown in Fig. S3(a) and the values listed in Table I. The interlayer distance between MoS_2 and different monolayers are in the range of 3.13-3.33Å, which is typical of vdW equilibrium spacing. Here we investigate the electronic structure of different MoS_2/BCN systems. The band structure, density of states (DOS) and projected (PDOS) of MoS_2/BCN are shown in Figs. 2(a-c). We can see that MoS_2/BC_3 is a semiconductor with a direct band gap of 0.4 eV, which compares with the band gaps of 0.7 eV and 1.26 eV of MoS_2 and BC_3 monolayers, respectively. We can see from the PDOS that the VBM and CBM are mainly derived from Mo atom (see Fig. 3 (b)). MoS_2/C_3N, has no band gap due to the strong interaction between C_3N and MoS_2, and the heterostructure is a metal. This result agrees with a previous report.[77] From the PDOS, we found that the metallic character near the Fermi level originates from Mo (see Fig. 3(b)). The MoS_2/C_3N_4 is a direct semiconductor with a band gap of 1.74 eV and the PDOS shows that both MoS_2 and C_3N_4 affect the electronic states near the Fermi level and there is a strong interaction between the two layers (see Fig. 3(c)).

Table I. The structural and electronic parameters of different MoS_2/BCN heterostructures shown in Fig. S3(a). The corresponding structural and electronic parameters including the lattice constants (a,b); the interlayer distance (D); the thickness (t) of MoS_2 (distance between two S atoms). The bond length between C-C atoms (d_{C-C}), B(N)-C ($d_{C-B(N)}$) atoms and Mo-S atoms; the buckling, defined by the difference between the largest and smallest z coordinates of atoms (Δz). All distance are given in Å. Electronic states (ES) are specified as metal (M) and semiconductor (SC). The band gap is shown in parenthe- ses and is given in eV.

Sys.	a	b	t	D	δz	$d_{C-B(N)}$	d_{C-C}	d_{Mo-S}	ES
BC_3	10.08	10.08	3.10	3.21	0.39	1.52	1.40	2.48	SC (0.4)
C_3N	9.72	9.72	3.16	3.33	0.0	1.40	1.40	2.44	M
C_3N_4	9.50	9.47	3.21	3.13	1.33	1.34-1.47	-	2.43	SC (1.74)

V. EFFECT OF ELECTRIC FIELD ON THE HETEROSTRUCTURES

Electrostatic gating is an effective way to tune the injection of carriers, the band structures and the electron redistribution in the heterostructure. The electronic band structure of the MoS_2/BCN heterostructures in the presence of a perpendicular electric field are shown in Figs. 5(a-c). The strength of electric field >0 (<0) denotes parallel (antiparallel) to the z-axis. It can be seen that the electric field can change the electronic structure of MoS_2/BC_3 significantly with a decrease in the band gap up (see Fig. 3(c)), and thus a semiconductor-to-metal transition occurs. The electric field dependence of MoS_2/C_3N is very different from the other two heterostructures and in this case, a negative electric field is able to open a band gap. When the applied negative electric field reaches -0.6 V/Å, and -0.8 V/Å, the band gap is 0.25 eV and 0.42 eV, respectively. We investigated that for the electric field varying from -0.8 to -1.2 V/Å, the band gap stays constant at $\sim$ 0.42 eV. In contrast, for MoS_2/C_3N_4, on applying an electric field, its band gap decreases for both for positive and negative electric field values. The band gaps are calculated 1.3 eV (at +0.2 V/Å), 0.8 eV (at +0.4 V/Å), 0.4 eV (at +0.6 V/Å). Interestingly, the band gap reaches 30 meV at +0.8 V/Å and for further increase of the electric field, a semiconductor-to-metal transition occurs. Notice that different heterostructures response differently to the applied external E-field. For example, the VBM of MoS_2/C_3N is dominated by MoS_2 layer, while the CBM originates from C_3N monolayer. In addition, given by Fig. 1, the VBM of MoS_2 is dominated by in-plane d-orbitals of the Mo atom while the CBM of C_3N is dominated by the p_z-orbitals of C atoms. Apparently, an applied out-of-plane electric field significantly affects C-p_z orbitals, while in-plane d-orbitals of Mo are slightly affected. In contrast, in the case of MoS_2/C_3N_4, both the VBM and CBM are affected by the applied field due to out-of-plane orbitals contributing to both band edges. Overall, depending on the atomic orbital characters of the band edges, the material response differently to the external effects. This electric field tuning of the band gaps, over a wide range for the MoS_2/BCN heterostructures are expected to lead to important applications in nanoscale electronic and optoelectronic devices.

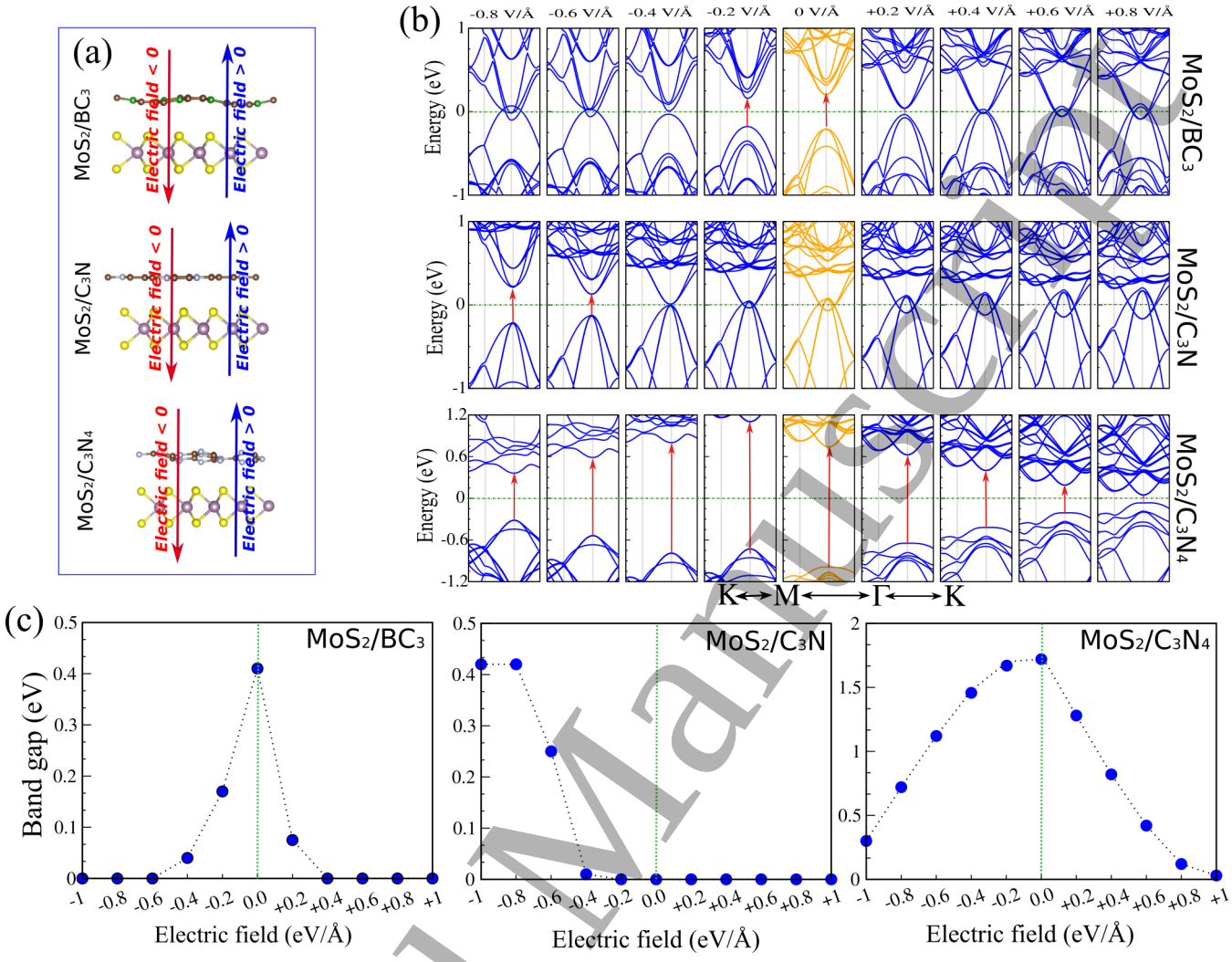

Figure 3. (a) Schematic view, (b) electronic band structure and (c) band gaps of MoS_2/BC_3, MoS_2/C_3N and MoS_2/C_3N_4 heterostructures with applied electric field. Electric field >0 and <0, denotes parallel and antiparallel to the z-axis, respectively. The zero of energy is set to the Fermi level energy.

VI. EFFECT OF STRAIN ON THE HETEROSTRUCTURES

Strain engineering is a robust method to tune the electronic properties and the topological nature.[79,80]

In the following, we explore the effect of strain on the electronic structure of MoS_2/BCN. The strain is defined as $\varepsilon = (a \pm a_0)/a_0 \times 100$, where a and a_0 are the strained and non-strained lattice constants, respectively, and the positive (negative) sign denotes tensile (compressive) strain. The electronic band structure under uniaxial strain are shown in Figs. 4(a-c). The schematic views of the heterostructures with applied strain are shown in Fig. S4. Our results show that MoS_2/BC_3, under -2% strain, is a semiconductor with a direct band gap of 0.3 eV, while the CBM and VBM are located at the Γ point. When compressive strain increases beyond -4%, the heterostructure transforms into a metal. Notice that the band gap disappears during the compression, the in-plane strain distorts the p-orbitals of C atoms which have contribution to the VBM of the heterostructure. We found that the direct band gap decreases with increasing tensile strain to 0.35 eV (at +2%) and 0.3 eV (at +4%). While for large strain (> + 6%) a direct-indirect band gap transition is predicted to occur. The values of band gaps are determined to be 0.25 eV (at +6%) and 0.15 eV (at +8%). We see that MoS_2/C_3N, under large uniaxial strain, remains metallic.

Our result show that MoS_2/C_3N_4 heterostructure under uniaxial strain for larger magnitudes of +2% (tensile) the energy band gap be decreases from 1.4 eV, (at +4%) to 1.1 eV (at +8%). Interestingly, we found that when the tensile uniaxial strain surpasses the critical value of +6%, the direct band gap of the heterostructure changed to indirect. Similar to the tensile strain case, for compression strain the band gap decreases from 1.25 eV (at -4%)

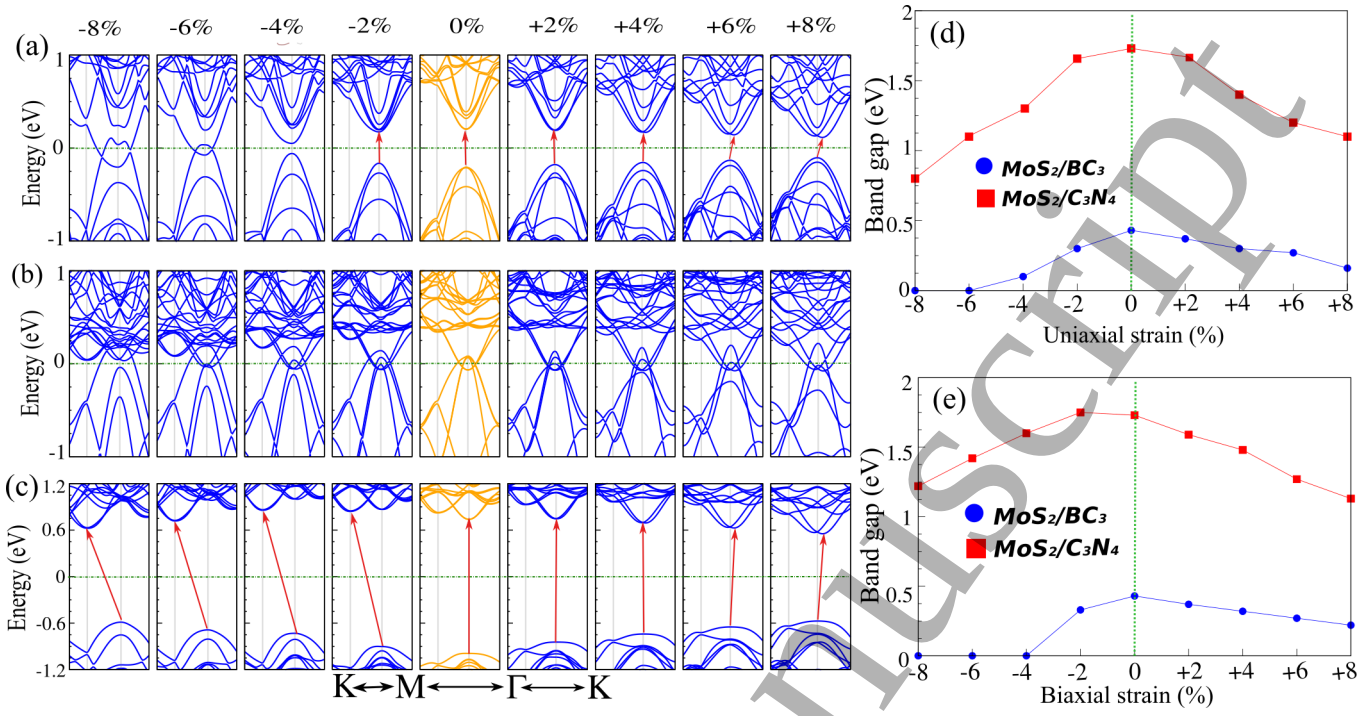

Figure 4. Electronic band structure of (a) MoS_2/BC_3, (b) MoS_2/C_3N and (c) MoS_2/C_3N_4 heterostructures under uniaxial strain. The zero of energy is set to the Fermi level energy. Band gap variation with (d) uniaxial strain and (e) biaxial strain.

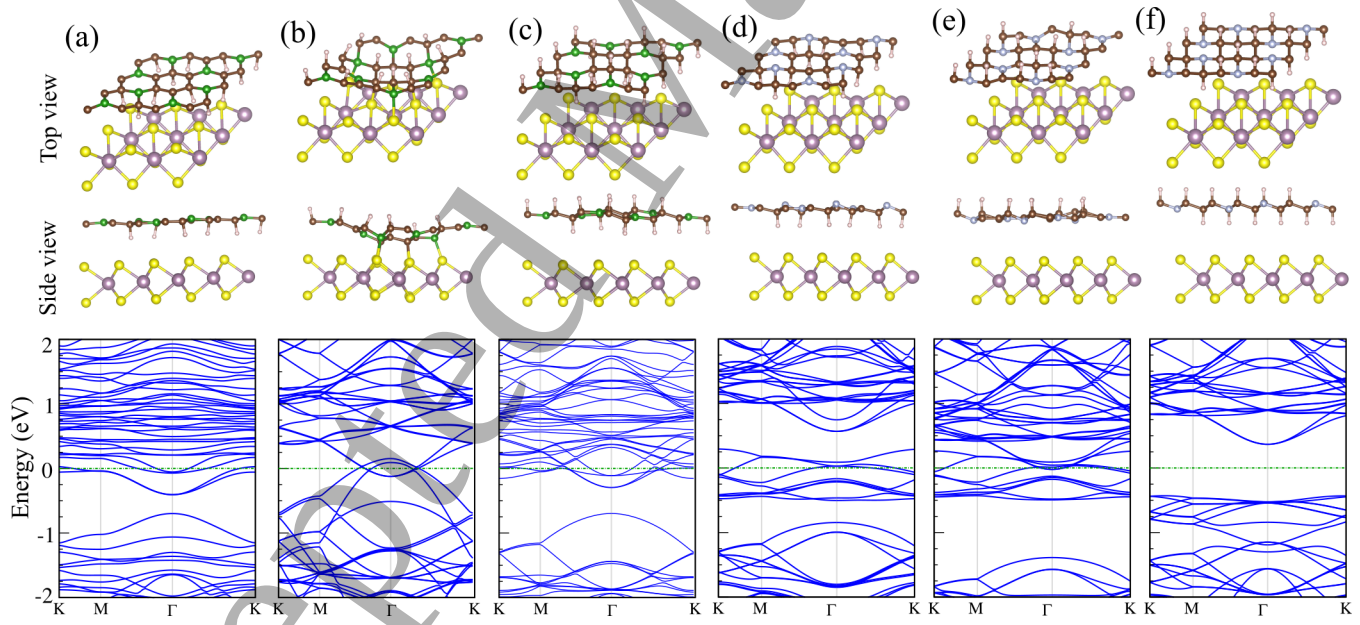

Figure 5. Optimized atomic structures of (a,b) semi- and (c) fully-hydrogenated MoS_2/BC_3. Optimized atomic structures of (d,e) semi- and (f) fully- hydrogenated of MoS_2/C_3N. Electronic band structure of both structures are shown in the bottom panels. The zero of energy is set to the Fermi level energy.

to 0.8 eV (at -8%) and we can see a direct-to-indirect band gap transition occurs and the VBM and CBM are located at Γ and M points, respectively. The variations of band gap with respect to both strains are shown in Figs. 4(d,e), while the electronic band structure of MoS_2/BCN under a biaxial strain are shown in Fig. S4.

It is found that MoS_2/BC_3 is initially a semiconductor with a 0.4 eV direct band gap. We see that with increasing biaxial strain from +2% to +8% the direct band gap decreases to 0.37 eV (at +2%), 0.32 eV (at

+4%), 0.26 eV (at +6%) and 0.2 eV (at +8%) and its semiconducting character is preserved. This situation is different for compression strain, so upon a biaxial strain -2% MoS_2/BC_3 is a semiconductor with a direct band gap of 0.2 eV. Interestingly, when the compressive strain reaches -4%, the heterostructure transforms into a metal and the metallic character is preserved for magnitude of strains larger than -4%. MoS_2/C_3N_4 is a semiconductor in the non-strained state and has a direct band gap of 1.7 eV. Our results show that with increase of magnitude biaxial strain from -2% to -4%, the band gap decreases from 1.75 to 1.6 eV and a direct-to-indirect band gap transition occurs. While for strain from -6% to -8%, an indirect-to-direct band gap transition with values of 1.42 eV and 1.2 eV, respectively, occurs. We can see that with increase of strain from +2% to +8%, the direct band gap changes to indirect and decreases with values of 1.6 (+2 %) to 1.1 eV (+8%). These results reveal strain engineering dependent band gaps and electronic state transitions in the MoS_2/BCN heterostructures, as well as the band gap changes between direct and indirect which could be of use in high-performance electronic and optoelectronic devices.

VII. HYDROGENATION OF ON THE HETEROSTRUCTURES

Adsorption of atoms on the surface of a structure can be an effective way to tune the properties of two-dimensional materials. We discuss here the modifications that occurs in the electronic properties by hydrogenation. We explore the structural and electronic properties of semi and full coverages of hydrogen atoms on MoS_2/BC_3 and MoS_2/C_3N heterostructures. After full optimization we found that hydrogen atoms adsorb on carbon atoms with bonds oriented normal to the BC_3 and C_3N planes. The optimized atomic structures of semi hydrogenated and fully hydrogenated MoS_2/BC_3 and MoS_2/C_3N are shown in top panel of Fig. 5. We consider two types of semi hydrogenated and are labeled theme as $SH1$ (when H atoms functionalize between two layers) and $SH2$ (when H atoms functionalize on top of BC_3 and C_3N layers), while fully hydrogenated labeled as FH. The structural parameters including bond length, interlayer distance and buckling are shown in Fig. S3(b) and the values are listed in Table II.

For semi and fully hydrogenated MoS_2/C_3N, there is a small increase of the lattice constant from 9.72 Å in MoS_2/BC_3, to 9.74 Å (semi) and 9.76 Å (fully). The increase in lattice parameter is due to the increase in bond lengths, which changes from 1.40 to 1.47 Å ($SH1$, $SH2$) and 1.52 Å (FH). The buckling for semi and fully hydrogenated are calculated in the range of 0.47-0.62 Å, while, the C-H bond lengths are 1.14 Å ($SH1$) and 1.15 Å ($SH2$) and 1.11 Å (FH). In general, the C-C and C-N bond lengths without hydrogenation are smaller compared to those between the N and C atoms

Table II. The structural and electronic parameters of different semi- and fully-hydrogenated MoS_2/BCN heterostructures shown in Fig. S3(b). Semi hydrogenated is labeled as $SH1$ (when H atoms functionalize between two layers) and $SH2$ (when H atoms functionalize on top of BC_3 and C_3N layers), while fully hydrogenated is labeled as FH. The corresponding structural and electronic parameters including the lattice constant (a); bond length between C-C atoms (d_{C-C}); the bond length between C-N atoms (d_{C-N}); the bond length between H atom and the nearest-neighbor C atom (d_{H-C}); the interlayer distance of between the H and S atom (D); the buckling, defined by the difference between the largest and smallest z coordinates of atoms (Δz). All distance are given in Å. Electronic states (ES) are specified as semi-metal (SM) and semiconductor (SC). The band gap is shown in parentheses and is given in eV.

Sys.	a	d_{C-C}	$d_{C-B,N}$	d_{H-C}	D	Δz	ES
MoS_2/BC_3 ($SH1$)	10.26	1.45	1.50	1.15	2.79	0.62	M
MoS_2/BC_3 ($SH2$)	10.15	1.55	1.61	1.12	2.04	1.66	M
MoS_2/BC_3 (FH)	10.26	1.45	1.50	1.15	2.26	0.22	M
MoS_2/C_3N ($SH1$)	9.74	1.48	1.47	1.14	2.71	0.59	M
MoS_2/C_3N ($SH2$)	9.72	1.47	1.38	1.15	3.40	0.62	M
MoS_2/C_3N (FH)	9.76	1.52	1.46	1.11	2.99	0.47	SC (0.9)

with one or both N and C atoms bonded to H atoms. The electronic band structure of semi and fully hydrogenated MoS_2/BC_3 and MoS_2/C_3N are shown in Figs. 5(a-f). In comparison to pristine MoS_2/BC_3, we can see that the electronic structure is modified due to the functionalization. We fund that a semiconducting behavior with band gap of 0.9 eV, where the VBM and CBM are located at K and Γ points. Our results show that impurity states appear around the Fermi-energy, and induce a metallic character. Interestingly, for the case of hydrogen atoms between two layers, the structure is strongly distorted and MoS_2 and BC_3 bond together and we can see a metallic characteristic as for the pristine MoS_2/BC_3 heterostructure. Notice, MoS_2/C_3N is a metal and the metallic character remains with semi hydrogenation. For fully hydrogenated MoS_2/C_3N, the system changes from a metal to semiconductor.

VIII. CONCLUSION

In summary, we performed an extensive study of the structural and electronic properties of a MoS_2 monolayer on BC_3, C_3N and C_3N_4 monolayers using first-principles calculations. The results show a wide variety of electronic properties which differ from the monolayers. Our results showed that MoS_2/BC_3 is a semiconductor with a direct band gap of 0.4 eV, while MoS_2/C_3N is a metal. In addition, MoS_2/C_3N_4 is a direct semiconductor with a band gap of 1.74 eV. The band structure of these heterostructures can be adjusted by application of an electric field and strain. MoS_2/BC_3, under -2% strain, is a semiconductor with a direct band gap of 0.3 eV and when uniaxial strain increases to larger than -4%, it transforms into a metal, and the metallic character is preserved for

strains larger than -6%. For large strain (> + 6%), a direct-indirect band gap transition occurs. MoS_2/C_3N remains metallic for all strain values considered. On application of an electric field the band gap of MoS_2/C_3N_4 decreases with increasing electric field. Interestingly, the band gap reaches 30 meV at +0.8 V/Å and with increasing electric field larger than +0.8 V/Å, a semiconductor-to-metal transition is occurs. We also investigate effects of semi and fully functionalization by H atom adsorption and found that the electronic properties are modified. The MoS_2/C_3N heterostructdure with fully hydrogenation transform from a metal to semiconductor. Tuning of the electronic structure in these ways leads to the potential exotic properties that could make such heterostructures of interest for future investigations and for applications in emerging technological devices with precisely controlled properties.

IX. CONFLICTS OF INTEREST

The authors declare that there are no conflicts of interest regarding the publication of this paper.

X. ACKNOWLEDGMENTS

This work has supported by the National Research Foundation of Korea(NRF) grant funded by the Korea government(MSIT)(NRF-2017R1A2B2011989).

* Bafekry.asad@gmail.com
† mitragh@skku.edu

[1] F. Bonaccorso, L. Colombo, G. Yu, M. Stoller, V. Tozzini, A. C. Ferrari, R. S. Ruoff, V. Pellegrini, *Sci.* 2015, **347**, 1246501.
[2] C. Tan, H. Zhang, *Nat. Commun.* 2015, **6**, 7873.
[3] B. Luo, G. Liu, L. Wang, *Nanoscale* 2016, **8**, 6904.
[4] C. Tan, X. Cao, X.-J. Wu, Q. He, J. Yang, X. Zhang, J. Chen, W. Zhao, S. Han, G.-H. Nam, M. Sindoro, H. Zhang, *Chem. Rev.* 2017, **117**, 6225.
[5] J. Di, J. Xiong, H. Li, Z. Liu, *Adv. Mater.* 2018, **30**, 1704548.
[6] H. Li , J. Wu , Z. Yin H. Zhang *Acc. Chem. Res.* 2014, **47**, 1067.
[7] W. Su , H. Dou , J. Li , D. Huo , N. Dai, L. Yang , *RSC Adv.* 2015, **5**, 82924.
[8] M. Buscema , G. A. Steele , H. S. J. van der Zant, A. Castellanos-Gomez, *Nano Res.* 2014, **7**, 561.
[9] W. Su , H. Dou , D. Huo , N. Dai, L. Yang, *Chem. Phys. Lett.* 2015, **635**, 40.
[10] S. Mouri , Y. Miyauchi K. Matsuda, *Nano Lett.* 2013, **13**, 5944.
[11] X. Zhou , W. Feng , S. Guan , B. Fu , W. Su, Y. Yao, *J. Mater. Res.* 2017, **32**, 2993.
[12] Y. Deng , Z. Luo , N. J. Conrad , H. Liu , Y. Gong , S. Najmaei , P. M. Ajayan , J. Lou , X. Xu, P. D. Ye, *ACS Nano* 2014, **8**, 8292.
[13] J. Yan , Y. Hao , Y. Cui , J. Zhang , Y. Zou , W. Zhang , G. Yu , J. Zheng , W. Xu, D. Zhu, *J. Mater. Chem. C* 2018, **6**, 12976.
[14] K. H. Chan , S. M. Ng , H. F. Wong , C. W. Leung, C. L. Mak, *Phys. Status Solidi A* 2019, **216**, 1800829.
[15] H. Yanagisawa, T. Tanaka, Y. Ishida, M. Matsue, E. Rokuta, S. Otani, C. Oshima, *Phys. Rev. Lett.* 2004, **93**, 177003.
[16] H. Tanaka, Y. Kawamata, H. Simizu, T. Fujita, H. Yanagisawa, S. Otani, C. Oshima *Solid State Commun.* 2005, **136**, 22.
[17] H. Yanagisawa, T. Tanaka, Y. Ishida, M. Matsue, E. Rokuta, S. Otani, C. Oshima, *Phys. Rev. B* 2006, **73**, 045412.
[18] J. Kouvetakis, R. B. Kaner, M. L. Sattler, N. Bartlett, *J. Chem. Soc. Chem. Commun.* 1968, **24**, 1758.
[19] K. S. Novoselov, D. Jiang, F. Schedin, T. J. Booth, V. V. Khotkevich, S. V. Morozov, A. K. Geim, *PNAS* 2005, **102**, 10451.
[20] D. Tomanek, R. M. Wentzcovitch, S. G. Louie, M. L. Cohen, *Phys. Rev. B* 1988, **37**, 3134.
[21] T. Sasaki, M. Akaishi, S. Yamaoka,Y. Fujiki, T. Oikawa, *Chem. Mater.* 1993, **5**, 695.
[22] A. Bafekry, S. Farjami Shayesteh, M. Ghergherehchi, F. M. Peeters, *J. Appl. Phys.* 2019, **126**, 144304.
[23] Y. Ding, Y. Wang, J. Ni, *Appl. Phys. Lett.* 2009, **94**, 073111.
[24] J. Mahmood, E. K. Lee, M. Jung, D. Shin, H. J. Choi, J. M. Seo, S. M. Jung, D. Kim, F. Li , M. S. Lah, N. Park , H. J. Shin, J.H. Oh, J. B. Baek, *PNAS* 2016, **113**, 7414.
[25] A. Bafekry, S. F. Shayesteh, F. M. Peeters, *J. Phys. Chem. C.* 2019, **123**, 12485.
[26] M.B. Tagani, *Comput. Mater. Sci.* 2018, **153**, 126.
[27] A. Bafekry, M. Ghergherehchi, S. Farjami Shayesteh, F.M. Peeters, *Chem. Phys.* 2019, **526**, 110442.
[28] A. Bafekry, C. Stampfl, S. Farjami Shayesteh, F. M. Peeters, *Adv. Elec. Mater.* 2019, doi:10.1002/aelm.201900459.
[29] M.B. Tagani, S.I. Vishkayi, *J. Appl. Phys.* 2018, **124**, 084304.
[30] A. Bafekry, S. Farjami Shayesteh, F.M. Peeters, *Phys. Chem. Chem. Phys.* 2019, **21**, 21070.
[31] A. Bafekry, C. Stampfl, S. Farjami Shayesteh, *ChemPhysChem* **21**, 164.
[32] M.D. Esrafili, S. Heydari, *Theor. Chem. Acc.* 2019, **138**, 57.
[33] O. Faye, T. Hussain, A. Karton, J. Szpunar, *Nanotech.* 2018, **30**, 75404.
[34] A. Bafekry, C. Stampfl, M. Ghergherehchi, S. Farjami Shayesteh, *Carbon* 2020, **157**, 371.
[35] Zh. Guizhi, L. Kun, S. Qiang, K. Yoshiyuki, J. Puru, *Comput. Mater. Sci.* 2014, **81**, 275.
[36] X. Li, S. Zhang and Q. Wang, *Phys. Chem. Chem. Phys.* 2013, **15**, 7142.
[37] S.I. Vishkayi, M.B. Tagani, *Nano-micro letters* 2018, **10**, 14.
[38] A. Bafekry, C. Stampfl, B. Akgenc, M. Ghergherehchi, *Phys. Chem. Chem. Phys.* 2020, **22**, 2249.

[39] S. I. Vishkayi, M.B. Tagani, *J. Phys. D: Appl. Phys.* 2020. doi=http://iopscience.iop.org/10.1088/1361-6463/ab7bb3.
[40] A. Bafekry, S. Farjami Shayesteh, F. M. Peeters, *J. Appl. Phys.* 2019, **126**, 215104.
[41] F. Ersan, O. Arslanalp, G. Gokoglu, E. Akturk, *Appl. Surf. Sci* 2014, **311**, 9.
[42] M. M. Oeid, *Appl. Surf. Sci* 2020, **508**, 144824.
[43] A. Bafekry, *Physica E: Low-dimensional Systems and Nanostructures* 2020, **118**, 113850.
[44] M. Yagmurcukardes, C. Sevik, F. M. Peeters, *Phys. Rev. B* 2019, **100**, 045415.
[45] F. Ersan, S. Cahangirov, G. Gokoglu, A. Rubio, E. Akturk, *Phys. Rev. B* 2016, **94(15)**, 155415
[46] A. Bafekry, C. Stampfl, B. Akgenc, B. Mortazavi, M. Ghergherehchi, Ch. V. Nguyen, *Phys. Chem. Chem. Phys.*, 2020. doi: https://doi.org/10.1039/D0CP00093K
[47] D. Kiymaz, M. Yagmurcukardes, A. Tomak, H. Sahin, R. T. Senger, F. M. Peeters, H. M. Zareie and C. Zafer, *Nanotechnology* 2016 **27**, 455604.
[48] C. Nguyen, H. Nguyen, *Chem. Phys.* 2016, **468**, 9.
[49] A. Bafekry, B. Akgenc, S. Farjami Shayesteh, B. Mortazavi, *Appl. Surf. Sci.* 2020, **505**, 144450.
[50] F. Ersan, S. Sarikurt, *Phys. Chem. Chem. Phys* 2019, **21(36)**, 19904-19914
[51] F. Iyikanat, M. Yagmurcukardes, R. T. Senger, H. Sahin, *J. Mater. Chem. C*, 2018, **6**, 2019.
[52] A. Bafekry, M. Neek-Amal, *Phys. Rev. B* 2020, **101**, 085417.
[53] Huynh V. Phuc, Tuan V. Vu, Nguyen N. Hieu, Victor .V. Ilyasov, Igor A. Fedorov, Bui D. Hoi, Le T. T. Phuong, Nguyen V. Hieu, E. Feddi, Chuong V. Nguyen, *J. Electronic Mater.* 2018, **47**, 4594.
[54] Z. Kahraman, A. Kandemir, M. Yagmurcukardes, H. Sahin, *J. Phys. Chem. C* 2019, **123**, 4549.
[55] A. Bafekry, C. Stampfl, F. M. Peeters, *Sci. Rep.* 2020, **10**, 213.
[56] M. M. Oeid, *Appl. Surf. Sci* 2020, **508**, 144824.
[57] Khang D. Pham, Nguyen N. Hieu, Le M. Bui, Huynh V. Phuc, Le T. N. Tu, Long G. Bach, Victor V. Ilyasov, Bin Amin, M. Idrees, Chuong V. Nguyen, *Chem. Phys. Lett.* 2019, **716** 155.
[58] B. Mortazavi, A. Bafekry, M. Shahrokhi, T. Rabczuk, X. Zhuang, *Materials Today Energy* 2020, **16**, 100392.
[59] M. Yagmurcukardes, S. Ozen, F. Iyikanat, F. M. Peeters, H. Sahin, *Phys. Rev. B* 2019, **99**, 205405.
[60] M. M. Obeid, H. R. Jappor, K. Al-Marzoki, D. M. Hoatc, T. V. Vu, S. J. Edrees, Z. M. Yaseen, M. M. Shukur, *Comput. Mater. Sci.* 2019, **170**, 109201.
[61] A. Bafekry, M. Ghergherehchi, S. Farjami Shayesteh, *Phys. Chem. Chem. Phys.* 2019, **21**, 10552.
[62] Tuan V. Vu, Nguyen V. Hieu, Le T. P. Thao, Nguyen N. Hieu, Huynh V. Phuc, H. D. Bui, M. Idrees, B. Amin, Le M. Duc, Chuong V. Nguyen, *Phys. Chem. Chem. Phys.* 2019, **21**, 22140.
[63] *Superlattice. Microst.* 2019, **130**, 545.
[64] A. Bafekry, B. Mortazavi, S. Farjami Shayesteh, *J. Magnetism and Magnetic Mater.* 2019, **491**, 165565.
[65] T. Ozaki, K. Nishio, H. Kino, *Phys. Rev. B* 2010, **81**, 035116.
[66] N. Troullier, J. Martins, *Phys. Rev. B* 1991, **43**, 1993.
[67] T. Ozaki, *Phys. Rev. B* 2003, **67**, 155108.
[68] T. Ozaki, H. Kino, *Phys. Rev. B* 2004, **69**, 195113.
[69] J. P. Perdew, K. Burke, M. Ernzerhof, *Phys. Rev. Lett.* 1996, **77**, 3865.
[70] Monkhorst, H. J. Pack, J. D. *Phys. Rev. B* 1976, **13**, 5188.
[71] T. Buko, J. Hafner, S. Lebgue and J. G. ngyn, *Phys. Chem. A* 2010, **114**, 118145.
[72] K. M. Mak, Ch. Lee, J. Hone, J. Shan, T. F. Heinz, *Phys. Rev. Lett.* 2010, **105**, 136805.
[73] Y. Ding, Y. Wang, J. Ni, *J. Phys. Chem. C* 2010, **114**, 12416.
[74] S. Behzad, *Surf. Sci.* 2017, **665**, 37.
[75] E. Kroke, M. Schwarz, E. Horath-Bordon, P. Kroll, Br. Noll and A. D. Norman, *New J. Chem.* 2002, **26**, 508.
[76] Q. Hu, Q. Wu, H. Wang, J. He and G. Zhang, *Physica Status Solidi (b)* 2011, **249**, 784-788.
[77] Y. Yang, Zh. Wang, *RSC Adv.*, 2019, **9**, 19837.
[78] H. J. Xiang, B. Huang, Z. Y. Li, S.-H. Wei, J. L. Yang and X. G. Gong, *Phys. Rev. X* **2**, 2012, 011003.
[79] K. P. Katin, K. S. Krylov, M. M. Maslov, V. D. Mur, *Diamond and Related Materials*, 2019, **100**, 107566
[80] I. Y. Sahalianov, T. M. Radchenko, V. A. Tatarenko, G. Cuniberti, Y. I. Prylutskyy, *J. Appl. Phys.* 2019, **126**, 054302.